Journal of Cultural Heritage 76 (2025) 277–287

Contents lists available at ScienceDirect

Journal of Cultural Heritage

journal homepage: www.elsevier.com/locate/culher

VSI: TechnoHeritage2024

Spectroanalytical approach for analysis of archaeological objects related to personal adornment from Teruel Museum

Laura Maestro-Guijarro[a,b,*], Pilar Punter[c], Francisco Javier Menasalvas[c], Ana Crespo[d], Santiago Sanchez-Cortes[d], Rafael Fort[e], Mónica Álvarez de Buergo[e], Paula María Carmona-Quiroga[f], Marta Castillejo[a], Mohamed Oujja[a]

[a] Instituto de Química Física Blas Cabrera, IQF-CSIC, C/ Serrano 119, 28006 Madrid, Spain
[b] Facultad de Ciencias Químicas, UCM, Pl. de las Ciencias, 2, 28040 Madrid, Spain
[c] Museo de Teruel, Pl. Fray Anselmo Polanco 3, 44001 Teruel, Spain
[d] Instituto de Estructura de la Materia, IEM-CSIC, C/ Serrano 123, 28006 Madrid, Spain
[e] Instituto de Geociencias, IGEO-CSIC-UCM, C/ Dr. Severo Ochoa 7, 28040 Madrid, Spain
[f] Instituto de Ciencias de la Construcción Eduardo Torroja, IETcc-CSIC, C/ Serrano Galvache 4, 28033, Madrid, Spain

ARTICLE INFO

Article history:
Received 25 February 2025
Accepted 20 October 2025
Available online 2 November 2025

Keywords:
Personal adornment objects
LIBS
p-XRF spectrometry
μ-Raman spectroscopy
Archaeological items
Teruel Museum

ABSTRACT

The immense variety of materials found in museum's archaeological collections often makes the tasks of cataloging and conservation difficult. This is even more challenging when dealing with objects related to personal adornments, such as jewelry or amulets, due to their extensive material diversity and complexity. For these reasons, the chemical characterization of this type of objects is crucial for linking the use of certain raw materials in the production of artifacts with commercial and influential spheres. The present study aims at the non/micro-invasive material characterization of a set of heterogeneous personal adornment pieces from a wide chronological period (2nd BC – 18th AD centuries) belonging to the archaeology collection of the Teruel Museum, Spain. A multi-analytical approach, without sample taking, was applied involving Laser-Induced Breakdown Spectroscopy (LIBS), which allowed surface and in-depth elemental analysis of materials including the detection of trace elements. The LIBS results were complemented by using portable X-ray fluorescence spectrometry (p-XRF) and μ-Raman spectroscopy, which offered additional information on elemental and molecular surface composition, respectively, for accurate mineralogical identification. The analysis of the considered objects revealed the presence of a wide variety of both organic and inorganic materials that were used in the manufacturing processes, including red coral, black amber, glass, and iron, among others. This allowed for a comprehensive characterization and provided extensive details about the provenance and relative dating of the objects, information that will be useful in the elaboration of an updated catalog list and new conservation protocols for the archaeological collection of the Teruel Museum.

1. Introduction

Since ancient times diverse and heterogeneous materials have been used for the fabrication of personal adornment objects. Identifying these materials can provide information about the socioeconomic issues of the communities making these objects: from religious beliefs and social status signs to local manufacturing or commercial exchanges in the archaeological settlements. However, due to the most common heterogeneity of these objects, material identification is frequently challenging. Usually, archaeologists and museum conservators catalog the materiality of objects via organoleptic tests, and the extensive experience of these professionals provides close approximations. Nevertheless, this approach is frequently insufficient in case of uncommon or degraded materials, and therefore, using versatile and complementary analytical techniques could be the solution for cataloging vast and heterogeneous archaeological museum collections.

XRF spectrometry has been applied to the study of cultural heritage materials since the 50s due to its non-invasive and, some-

* Corresponding author.
E-mail addresses: lmaestro@iqf.csic.es (L. Maestro-Guijarro), ppunter@dpteruel.es (P. Punter), fjmenasalvasvalderas@dpteruel.es (F.J. Menasalvas), a.crespo.i@csic.es (A. Crespo), ssc@iem.cfmac.csic.es (S. Sanchez-Cortes), rafael.fort@csic.es (R. Fort), alvarezm@geo.ucm.es (M. Álvarez de Buergo), paulacq@ietcc.csic.es (P.M. Carmona-Quiroga), marta.castillejo@iqf.csic.es (M. Castillejo), m.oujja@iqf.csic.es (M. Oujja).

https://doi.org/10.1016/j.culher.2025.10.012

times, portable capability. This technique is based on the excitation of atoms of the material under study by an X-ray beam, resulting in secondary fluorescent emission. XRF intensity directly depends on the concentration of every element in the specimens. Generally, it is used to determine the concentrations of elements from aluminum ($Z = 13$) to uranium ($Z = 92$) [1]. The quantitative results given by this technique are immediate and easy to understand. For archaeological objects, surface analysis gives details on the nature of the soils where the objects were buried, the composition of degradation layers (i.e. glass or metals), the presence of protective coatings, etc. XRF penetrates a few µm from the surface at low energies and several mm at high energies, allowing better detection limits (10 – 50 ppm) depending on the elements, beam collimator size, and detector type [2]. Thus, the information provided is highly valuable in archaeometric studies by allowing linking the object with a specific archaeological site or identifying earlier conservation interventions. Nonetheless, its limitation in detecting trace or light elements (chromophores or impurities), especially in unpolished archaeological samples [3–5], could be a drawback that could be compensated by its combination with complementary analytical techniques. In that respect, the use of XRF with other techniques, such as LIBS, has been proven helpful in determining the material composition of archaeological objects [6–8].

The versatility of the LIBS technique is considered an asset for identifying numerous materials used in cultural heritage [6,9–13], especially those of archaeological nature. LIBS is based on focusing a pulsed laser power on a sample surface to ablate a small amount of material. The spectrum of the light-emitting-induced plasma reveals qualitative and semi-quantitative information about the elemental sample composition. Despite its micro-invasive character, no sample pretreatment is needed and its application to the study of inorganic materials, commonly present in archaeological collections such as glass, stone, pottery, metal, etc., barely causes noticeable damage. Usually, a small crater of about tens of micrometers wide and a few microns deep per laser pulse is left on the surface of the object. Moreover, LIBS allows in-depth analysis of the substrate by collecting the spectra of the emission caused by the application of successive laser pulses on the same spot. Considering the common burial condition of the archaeological objects, this feature of LIBS allows the analysis of the bulk material, without the interference of signals from superficial deposits or degradation layers. LIBS is also a highly sensitive technique for the detection of light elements that can be present as traces or impurities, such as hydrogen (H), lithium (Li), boron (B), carbon (C), and oxygen (O) [14].

Another analytical technique, extensively used since the 1980s to analyze different cultural heritage materials is μ-Raman spectroscopy, which provides specific molecular fingerprints of core materials in a non-invasive and non-destructive way. Based on inelastic scattering and the generation or annihilation of elementary excitations during the interaction between monochromatic light (laser) and matter, Raman spectroscopy induces transitions between vibrational and rotational energy levels, offering detailed structural information about the material. This technique has been applied for the characterization of pigments, minerals, or gemstones and is particularly useful for identifying corrosion or degradation agents, as well as organic materials, like textile fibers, colorants, protective coatings, etc. [15,16].

The present work undertakes the investigation of fifteen archaeological objects spanning various historical periods (from the 2nd BC to 18th AD centuries) found in seven distinct settlements in the Teruel province of Spain. These artifacts, housed in the archaeological collection of the Teruel Museum, exhibit a wide range of materials and manufacturing techniques. Despite this variability, they are all linked by their function as personal adornments. A multi-analytical approach involving LIBS, portable X-ray fluorescence spectrometry (p-XRF), and µ-Raman spectroscopy techniques has been used. Owing to the complementarity of these techniques, this approach allowed the surface and in-depth analysis of the composition of the materials under consideration through the detection of trace or minor elements (LIBS), the characterization of surface deposits or degradation layers in a semi-quantitative way (p-XRF) and the identification of minerals or mineraloids/organic compounds (μ-Raman spectroscopy).

2. Research aim

The present work aims to provide a feasible and useful in situ multi-analytical approach for museum conservators to characterize their collections for a correct cataloging task, using a combination of non/micro-invasive techniques such as LIBS, p-XRF and µ-Raman spectroscopy without the requirement of sampling or sample preparation. The combination of these techniques allowed for overcoming the complexity of the thick layers covering the archaeological objects, consisting in corrosion products and deposits from the burial environment. While p-XRF and micro-Raman helped answering inquiries associated with elemental and molecular surface composition of the archaeological pieces, LIBS solved questions about their core composition and manufacturing techniques employed for their production. The present approach is particularly valuable due to its non/micro-invasive nature and the availability of portable instrumentation for conducting in situ analysis of personal adornments. The data obtained from the application of the three techniques, together with those generated by historical studies, provided a better understanding of the manufacturing techniques employed, the availability of raw materials, and the political and social circumstances, thus facilitating complete cataloging and characterization of the considered archaeological objects related to personal adornment from Teruel Museum.

3. Materials and methods

3.1. Description of the objects

The present work is based on the analysis of a set of different archaeological objects from a collection belonging to the Provincial Museum of Teruel, NE Spain. Opened in 1959, with the purpose of promoting the cultural heritage of Teruel province, it houses collections devoted to archaeology, ethnography, and art, with its archaeological collection being the largest and most significant [17].

The small objects of the set (Fig. 1) span a broad chronological range (2nd BC – 18th AD centuries) and have unequal materiality. However, their common characteristics lie in their use as personal adornment or apotropaic objects (i.e. objects that are believed to have the power to avert evil or harm). These pieces were unearthed at seven different archaeological sites, all located along the province of Teruel (Aragón region, Spain). Some of them are declared Assets of Cultural Interest, the greatest protection granted by the Spanish State. The objects are organized and cataloged in Table 1 according to date.

The first six items (Fig. 1, **1a – 1f**) come from *La Caridad*, a Roman military site built *ex-novo* in Caminreal village. *La Caridad* was a settlement with a brief occupation period (late 2nd – 1st last third centuries BC) serving as an administrative and economic center for territorial structuring, at this time closely linked to the iron mining operation of Sierra Menera [18]. The group of elements from this archaeological site related to personal adornment is not very abundant, although it includes two rings (Fig. 1, **1a** and **1b**), two cabochons (Fig. 1, **1c** and **1f**), an amulet (Fig. 1, **1d**), and a bead (Fig. 1, **1e**).

Two intaglios were found in *El Palao*, one showing a figure holding a lyre, apparently Apollo (Fig. 1, **2a**), and the other fea-

Fig. 1. Images of the archaeological objects for personal adornment considered in the present work.

Table 1
Archaeological information about the set of personal adornment objects. The information was provided via the Teruel Museum catalog. All the archaeological sites marked with an asterisk (*) are declared Asset of Cultural Interest by the Spanish State.

Archaeological site	Chronology	Typology	Cultural environment
La Caridad site (Caminreal) *	Late 2nd century BC – last third of 1st century BC	**1a** Ring **1b** Ring **1c** Cabochon **1d** Amulet **1e** Bead **1f** Cabochon	Roman City. Late Republican Period
Ibero-Roman settlement of *El Palao* (Alcañiz) *	2nd century BC – 1st century AD	**2a** Intaglio **2b** Intaglio	Roman city
Roman Villa of *La Loma del Regadío* (Urrea de Gaén) *	3rd – 4th centuries	**3a** Intaglio **3b** Bead	Roman Villa. Late Imperial Period
Hermitage of *La Virgen de la Peña* (Berge)	Late 6th century	**4a** Bead **4b** Bead	Necropolis around the Hermitage
Mausoleum of *Los Amantes de Teruel* (Teruel)	13th century	**5** Bead	Urban area. Middle ages
Jewish necropolis of Teruel (Teruel)	15th – 16th centuries	**6** Bead	Hills surrounding the city. "Planos de Santa Lucía"
San Juan Bautista Chapel (Bañón)	18th century	**7** Button	–

turing a human bust profile (Fig. 1, **2b**). *El Palao,* an Ibero-Roman settlement in Alcañiz, was the main urban settlement of the central area of Lower Aragón from the 2nd century BC until the 1st century AD. Its elevated orographic condition allowed control over the surrounding territories. However, it does not follow the typical Roman urban layout, possibly due to the coexistence of the Iberian native population of whom signs of its activities were also found [19].

A greenish intaglio (Fig. 1, **3a**), and a black bead (Fig. 1, **3b**) were found in the Roman Villa of *La Loma del Regadío*. Although the site's occupation spanned from the 1st to the 5th century AD, both pieces are from the late period (3rd – 4th centuries AD). The late *villa* results from an intense structural distribution refurbishment with the aim of oil and wine production, the principal activity of the settlement [20].

Among other grave goods (belt buckles, pendants, bronze rings, etc.) of the necropolis around the Hermitage of *La Virgen de la Peña*, two beads (Fig. 1, **4a** and **4b**) were discovered during the archaeological excavations of 1987. In contrast with the Roman sites, the documentation of the Late Antiquity is less extensive [21].

One black bead (Fig. 1, **5**) was found in *Los Amantes de Teruel* Mausoleum. This bead was part of a female funerary trousseau, consisting of a necklace of 25 pieces; except for this one, the remaining 24 are made of bone. The burial site appeared during the *Mausoleo de Los Amantes* archaeological excavation, in the context of a 13th-century Christian necropolis, attached to the old Church of San Pedro, in Teruel.

Another black bead (Fig. 1, **6**) was unearthed in the Jewish necropolis of Teruel, in the hills surrounding the city, an area commonly called *Altos de Santa Lucía*. This bead is part of the grave

Table 2
Semi-quantitative elemental composition in (wt %) of the archaeological objects as determined by p-XRF. *Bal value is the difference to 100 % of the sum of all measured elements.

Sample	Ba	Sb	Sr	Pb	Cu	Fe	Mn	Cr	V	Ti	Ca	K	Al	P	Si	Cl	S	Bal*
1a Head	–	–	–	–	–	10.0	–	–	–	0.1	1.4	0.4	1.0	–	9.1	0.1	0.2	77.7
1a Shank	–	–	–	–	–	96.9	–	–	–	–	–	–	–	0.1	2.6	–	0.4	–
1b Head	0.1	0.1	0.1	0.6	–	17.5	0.5	–	–	–	3.9	0.2	0.8	–	7.8	0.1	0.3	68.0
1b Shank	–	–	–	–	–	95.9	–	–	–	0.1	–	–	–	–	3.4	–	0.6	–
1c	–	–	–	–	–	–	–	–	–	–	0.3	0.1	–	–	0.1	–	0.6	98.9
1d	0.8	–	–	–	–	30.9	–	–	–	0.2	13.8	1.4	3.5	0.1	13.9	0.3	0.3	34.8
1e	–	–	0.2	–	–	0.9	–	–	–	–	20.7	0.3	0.5	–	2.5	–	0.6	74.3
1f	0.1	0.2	–	–	–	0.2	0.8	–	–	–	4.5	0.4	1.7	–	29.5	0.5	0.2	62.0
2a	–	–	–	–	–	0.1	–	–	–	–	0.6	0.1	0.6	0.1	43.5	0.1	0.3	54.6
2b	–	–	–	–	–	0.1	–	–	–	–	–	–	–	–	37.9	–	–	62.0
3a	–	–	–	–	–	0.1	–	0.1	0.1	–	0.2	0.5	5.7	8.8	6.0	0.1	0.1	78.3
3b	–	–	0.1	–	–	–	–	–	–	0.1	4.5	1.0	–	–	0.5	0.3	2.5	91.0
4a	–	–	–	–	0.1	–	–	–	–	–	0.3	–	0.1	–	0.5	–	0.2	98.8
4b	–	–	–	0.1	0.1	–	–	–	–	–	1.4	0.1	0.2	0.1	0.8	–	0.4	96.8
5	–	–	–	–	–	0.3	–	–	–	–	1.5	–	–	–	0.1	–	0.5	97.6
6	–	–	–	–	–	0.6	–	–	–	–	–	–	–	–	0.1	0.1	2.6	96.6
7	–	–	–	–	–	–	–	–	–	–	1.2	–	–	–	0.1	–	1.4	97.3

goods found during the 1926 excavations [22]. The report on these dates described it as: “Ten black necklace beads of varying thickness, parallel circles carved on it. Perhaps made of black amber” [23].

The last object (Fig. 1, **7**) is a button of a similar material as the previous one. This piece comes from the subsoil of the Parish Church of *San Juan Bautista*, built between 1692 and 1701, in the town of Bañón. During archaeological works in 2009, this piece was found in a burial site, near glass and ceramic objects dating from the 18th century.

3.2. Analytical techniques

The set of archaeological objects was compositionally analyzed using the techniques of p-XRF spectrometry, LIBS, and μ-Raman spectroscopy.

X-ray fluorescence (XRF) analyses were carried out using a portable THERMO NITON XL3T EDXRF device, which is equipped with an X-ray tube operating at 50 keV and 100 μA, along with a geometrically optimized large Si drift detector (GOLDD). This setup enables rapid, non-destructive elemental measurements on-site in various fields, including metal identification and soil analysis. The objects being analyzed are placed in a large sampling platform that shields the operators from X-rays, while proper positioning of the samples is achieved using a CCD camera. The analyses were performed directly on the surfaces of the objects without any prior preparation. Two factory calibration modes, referred to as Mining (M) mode and Soils (S) mode, are available for these measurements. For this study, all measurements were conducted using the M calibration mode, which allows the detection of elements such as Ba, Sn, Cd, Pd, Ag, Mo, Nb, Zr, Sr, Bi, As, Se, Hg, W, Pb, Zn, Cu, Ni, Co, Fe, Mn, Cr, V, Ti, Ca, Cl, K, S, P, Si, and Al. In the present study, each analysis involved a 70-second exposure, with a 3 mm diameter measurement area, and the database used for peak assignment was the Cu-Zn Mining database. However, for the metal ring objects, the exposure time was 30 s, the measurement diameter was 8 mm, and the Metals database was used for peak assignment. Additionally, XRF, unlike other techniques like LIBS, cannot detect light elements with an atomic number (Z) below 13 (e.g., Na, Mg, B, C). Therefore, the content of organic matter (C, N, O, H) and light elements (Be, B, F, Na) in the analyzed samples is beyond the scope of this technique. Nonetheless, the Mining measurement method provides a result called “Bal” (balance), which corresponds to the difference, up to 100 wt %, that has not been assigned to other elements [24]. These limitations render XRF a semi-quantitative technique for analyzing the considered objects.

LIBS analyses were performed with a Q-switched Nd:YAG laser (15 ns pulses, 1 Hz repetition rate) operating at 266 nm (4th harmonic). The laser beam was conducted and focused on the sample surface at the angle of 45° by using a dichroic mirror system and a 15-cm focal length lens used to reach the threshold laser ablation of the materials. The laser fluence of 3.5 J/cm^2 (resulting in a crater with a diameter of 200 µm and a depth of around 10 µm) was used to achieve an optimal signal/noise relation, to get a real fingerprint of the elemental composition of the analyzed samples and to preserve their integrity. Cut-off filters of 300 and 330 nm were placed at the entrance slit of the spectrograph to reduce the scattered excitation laser light and to avoid second-order diffraction. The LIBS spectra were collected in the wavelength range between 250 and 600 nm using a detection system based on an intensified charge-coupled device (ICCD) camera from Andor Technology (iStar CCD 334, 1024 × 1024 active pixels, 13 μm × 13 μm pixel size) coupled to an 0.2 m spectrograph (Andor, Shamrock Kymera-193i-A), equipped with a diffraction grating of 1800 grooves/mm. For each considered sample, LIBS spectra we collected from different areas resulting in similar qualitative results.

The molecular composition of the materials was analyzed using μ-Raman spectroscopy via a Renishaw Raman InVia Reflex spectrometer equipped with two excitation wavelengths at 532 nm (Nd:YAG laser) and 785 nm (diode laser). The spectra were acquired during 10-s exposure time, with 1 accumulation and laser power up to 5 mW. The acquisition spectra range was 100 – 3000 cm^{-1} with a spectral resolution of 4 cm^{-1}.

4. Results and discussion

4.1. p-XRF spectrometry

The set of personal adornment objects was analyzed by p-XRF spectrometry to provide semi-quantitative measurements of their elemental composition. Table 2 shows the chemical composition in wt % of the studied archaeological pieces. As mentioned, this technique penetrates a few µm at low energies, hence, detecting the composition of the surface and/or core of the material may vary based on the nature of the object. Moreover, in light of the buried condition of these pieces, the Bal number (as defined in Section 3.2.) could be higher in some cases, probably due to the presence of remaining organic matter (C, nitrogen (N), O, H) or light elements, such as B, Li, or sodium (Na), that cannot be detected with p-XRF technique.

Concerning the shanks of the rings (Fig. 1, **1a** and **1b**), almost 100 wt % is detected as Fe (Table 2). The manufacturing of these

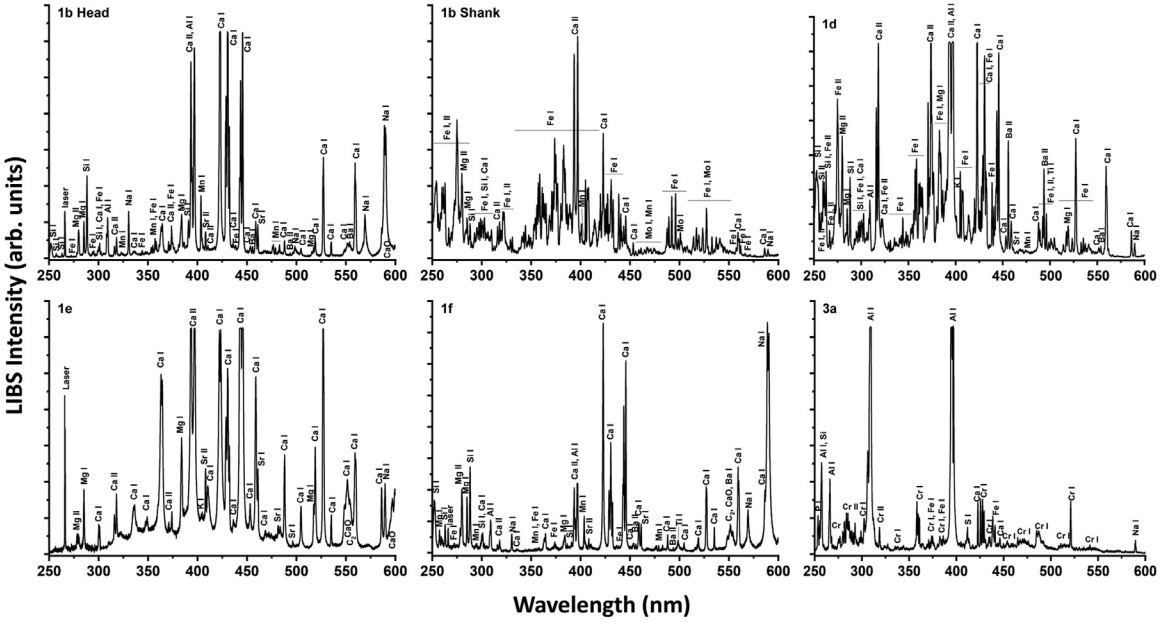

Fig. 2. LIB spectra of head and shank areas of **1b**, **1d**, **1e**, **1f**, and **3a** objects. The assigned neutral (I) and ionic (II) atomic lines are indicated.

iron objects could be tightly related to the already mentioned exploitation of Sierra Menera mines and the metallurgical industry of this settlement [18]. The heads of these two rings present between 68.0 and 77.7 wt % of undetermined elements, despite the relevant calcium (Ca) and silicon (Si) content, and 10 to 17.5 wt % of iron (Fe). The latter could be related to the advanced state of degradation of the shanks of both rings.

Cabochon of the same site (Fig. 1, **1f**), presents a composition richer in silica, with the presence of Ca, aluminum (Al), and some minor elements such as manganese (Mn), chlorine (Cl), potassium (K), antimony (Sb), or barium (Ba) (Table 2). Moreover, like in heads of the rings **1a** and **1b**, (Fig. 1) it is important to note the high percentage of undetected elements, 62.0 wt %, possibly associated with the presence of an organic coating applied during a previous restoring intervention.

Object **1d** (Fig. 1) is another item with considerable iron content (30.9 wt %). Nonetheless, the p-XRF analysis of this amulet reveals an extensive presence of Ca (≈ 14 wt %), Si (≈ 14 wt %), Al (≈ 4 wt %), and in smaller proportions: K, Ba, Cl, sulphur (S), and titanium (Ti), with a Bal value of around 35 wt %.

The p-XRF results for the cabochon **1c**, beads **3b, 4a, 4b, 5**, and **6**, and button **7** yield Bal values of nearly 100 wt % due to the probable reason of being made entirely of organic material. A similar case is for the bead **1e**, with a high content of Ca, and the presence of Si, Fe, and S, but with a Bal number around three-quarters of its total wt %.

Intaglios **2a** and **2b** from the *El Palao* Ibero-Roman site are mainly constituted by Si (43.5 wt % and 37.9 wt %, respectively) and half of its total wt % of undetected elements. Finally, the greenish **3a** intaglio exhibits an unusual chemical composition, characterized by high wt % of phosphorus (P), Al, and Si.

4.2. LIBS

LIBS measurements were carried out to complement the results on the chemical elemental composition of the objects studied via p-XRF. Representative spectra are displayed in Fig. 2 and Fig. 3 showing the assignment of the spectral lines based on the data from the NIST database [25]. Table 3 summarizes the derived elemental composition of all the pieces analyzed. The LIBS results

Table 3
Elemental composition of the objects of personal adornment from Teruel museum as determined by LIBS. The main components are indicated in bold.

Sample	Elemental Composition as Determined by LIBS
1a Head	Ba, **Mo**, Sr, **Fe**, Mn, **Ca, Si**, Al, Mg, Na
1a Shank	Ba, Mo, Sr, **Fe**, Mn, Ca, Na
1b Head	Ba, Sr, Fe, **Mn, Ca**, CaO, **Si**, Al, **Mg, Na**
1b Shank	**Mo, Fe**, Mn, Ca, Si, Mg, Na
1c	Sn, Sr, Cu, Fe, Ca, Si, Al, Mg, **Na, CN, C_2**, C
1d	**Ba**, Sr, **Fe**, Mn, Ti, **Ca**, K, **Si**, Al, Mg, Na
1e	**Sr, Ca, CaO**, K, **Mg**, Na, C_2
1f	Ba, Sr, Fe, **Mn**, Ti, **Ca**, CaO, **Si**, Al, **Mg, Na**, C_2
2a	Fe, Ca, **Si**, Na
2b	Fe, Ca, **Si**, Na
3a	Fe, **Cr**, Ca, **P, S**, Si, **Al**, Na
3b	Sn, **Sr**, Cu, Fe, Cr, Ti, **Ca**, S, **Mg**, Na, **CN, C_2**, C
4a	Pb, Sn, Sr, Zn, **Cu**, Ni, Fe, Ca, Si, Al, Mg, Na, **CN, C_2**, C
4b	Pb, Sr, Zn, Cu, Fe, Ca, Si, Al, Mg, **Na, CN**, C_2, **C**
5	Sr, Fe, **Ca, CaO**, Mg, Na, **CN**, C_2
6	Sn, **Sr**, Cu, **Ca**, Mg, Na, **CN, C_2**
7	Sn, **Sr**, Cu, Fe, V, **Ca**, S, Al, Mg, Na, **CN, C_2**, C

agree well with those obtained by p-XRF (Table 2), although the comparison indicates the capacity of LIBS to detect more minor and/or trace elements.

Beginning with *La Caridad* objects, spectra of the shanks of both rings **1a** (spectrum not shown) and **1b** (Fig. 2, **1b Shank**) show intense lines of Fe, confirming the p-XRF results. In contrast, the spectrum of the amulet **1d** (Fig. 2, **1d**) shows, as the rings, intense emission lines of Fe, with additional lines of Ba, Ca and Si, indicating a more diverse elemental composition. These results suggest that the shanks of the rings **1a** and **1b** are a product of ironwork whereas the amulet **1d** is carved in iron ore.

Spectra of the heads of the rings **1a** and **1b** are rich in Ca, Si, magnesium (Mg), and Na (Fig. 2, **1b Head**). A similar composition is presented by cabochon **1f** although the presence of extra lines of Mn, K, and Al (Fig. 2, **1f**) indicates that the material of the decoration of **1f** is more complex than those of the heads of rings **1a** and **1b**

In what concerns cabochon **1c**, and beads **4a** and **4b**, LIB spectra revealed similar composition. These spectra (as an example see

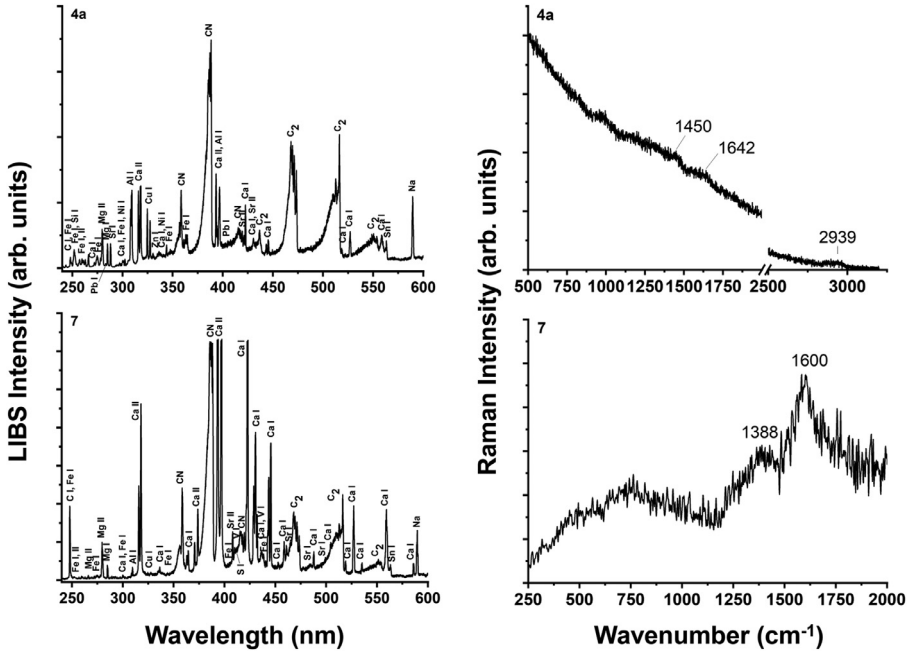

Fig. 3. Comparison of LIB and Raman spectra of **4a** (upper spectra), and **7** (lower spectra) objects. The assigned neutral (I) and ionic (II) atomic lines are indicated in LIB spectra.

Fig. 3**, 4a**) display Na lines with C_2 Swan bands around 473, 515, and 560 nm [26], indicative of the presence of a carbon-containing material. Aside from the C_2 bands, LIB spectra also contain intense CN bands (around 388, 415 nm) and atomic C lines. The latter is the result of the reaction of atomic C from the ablation plasma with environmental nitrogen (N) [27]. Nonetheless, the spectra of the two beads **4a** and **4b**, found around the Hermitage of *La Virgen de la Peña* also show the presence of lead (Pb), nickel (Ni), and copper (Cu), elements which may come from impurities provided by the soil of the burial environment or from the formation of the material itself.

LIB spectra of beads **3b, 5**, and **6**, and button **7** (Fig. 3, **7**) reveal a main composition based on C, with the same bands of C_2 and CN displayed in the case of **1c, 4a**, and **4b** objects. However, some minor elements such as strontium (Sr) or Fe were also detected, in agreement with the p-XRF analysis (Table 2). Owing to these results, it can be concluded that a carbon-based core is the main component for these objects.

Considering all LIBS results (Table 3, Fig. 3), it is evident that objects **1c, 3b, 4a, 4b, 5, 6**, and **7** are manufactured with carbon-based materials. In this context, considering the elements not directly determined by p-XRF analysis and represented as "Bal" numbers (Table 2), it can be inferred that these archaeological pieces (with Bal ranging from 91 to 99 wt %) are mainly composed of organic material.

The LIB spectrum of pinkish bead **1e** (Fig. 2**,** 1**e**) indicates a major presence of calcium, along with Mn and Sr (Table 3) as already revealed by p-XRF. Contrary to what is found by p-XRF, Si lines possibly indicative of a superficial deposit like sand, are not present in the LIB spectrum of this object. The presence of C_2 emissions, characteristic of a carbon-containing material is compatible with the XRF Bal number of around 74 wt %.

LIB spectra of **2a** and **2b** intaglios of the *El Palao* site contain spectral lines of Fe, Ca, Na, and intense ones assigned to Si (Table 3), which agree with p-XRF and suggest a composition based on a quartz mineral or similar silica-based material.

Finally, examining the LIB spectrum of the greenish intaglio **3a** found in the Roman Villa of *La Loma del Regadío* (Fig. 2, 3**a**), displays a high content of Al, chromium (Cr), and P. Emission lines from Si, Ca, S, and Fe are also present (Table 3), in agreement with p-XRF findings (Table 2). Upon comparison with the chemical composition of variscite ($AlPO_4{\cdot}2(H_2O)$) in the Handbook of Minerals [28] the main constituents are identified as P and Al oxides, along with water. Nevertheless, it is essential to highlight the presence of vanadium (V), Fe, and Cr oxides, which were also detected in object **3a** as revealed by the p-XRF analysis (Table 2), and corroborated by the LIBS results (Table 3). The chemical composition fits with the results given by other similar investigations of this gemstone (anciently called *Callais*) [29–31]. This mineral was valued by ancient societies, particularly the Romans, for its resemblance to a richer and odder material, the emerald. In this sense, Domínguez-Bella reports that "variscite was used, together with gold (Au), silver (Ag), and other materials such as red coral, pearls, and quartz, in the manufacture of jewels that had a circulation of thousands of kilometres in the Roman Empire" [30]. Nonetheless, further analyses, such as X-ray diffraction (XRD) [32] or Particle-Induced X-ray Emission (PIXE) [33], could provide additional information regarding the material characterization and the provenance of this object.

4.3. μ-Raman spectroscopy

μ-Raman spectroscopy measurements were also conducted to identify the specific molecular nature of the core materials of the archaeological pieces (Figs. 3 and 4). Comprehensive analyses (results are shown in Table 4) were performed on all samples although, from some of them, no Raman signal was detected at the used excitation wavelengths.

For cabochon **1f,** two Raman spectra were acquired in two different areas (Fig. 4, **1f**). As seen in the upper spectrum of this figure, two broad bands appear at around 570 and 1093 cm^{-1}, both attributed to amorphous silicate vibrations (Table 4). These bands correspond to SiO_4 tetrahedron bending and stretching vibrations respectively, typical fingerprints of glassy materials [45]. These two bands of glass are also present in the Raman spectrum of the head ring **1b** (not shown), indicating that this ring decoration is made of glass paste, as supported by the previous LIBS and p-XRF analyses.

Furthermore, the lower Raman spectrum of **1f** in Fig. 4 displays bands at 1731, 1450, and 1113 cm^{-1}, corresponding to νC=O,

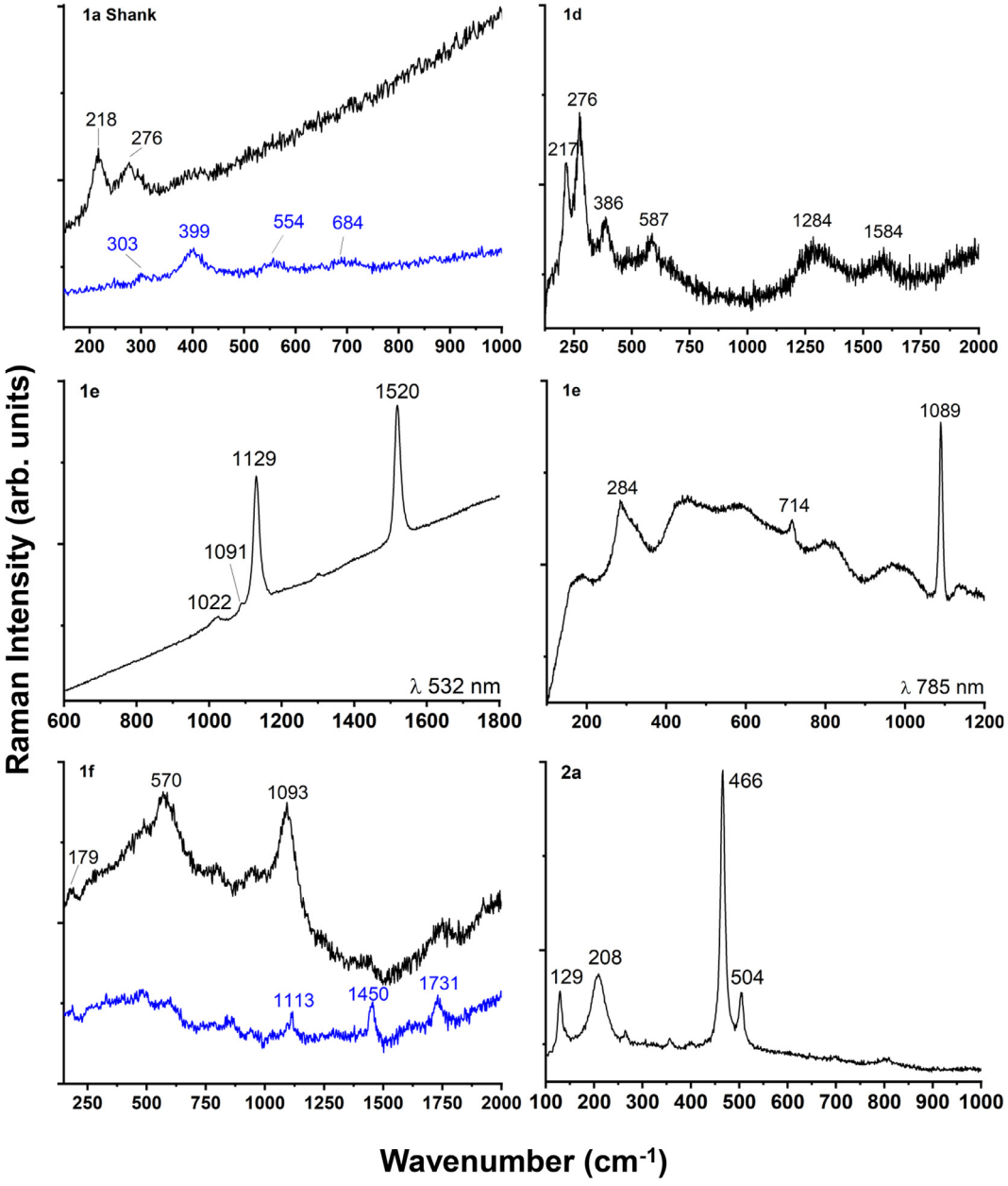

Fig. 4. μ-Raman spectra from samples **1a** shank and **1d** obtained with 532 nm laser excitation (upper raw). Comparative Raman spectra from sample bead **1e** were acquired using 532 nm (left) and 785 nm (right) excitation wavelengths (middle raw). Raman spectra of **1f** in two different glass areas at 532 nm, and item **2a** spectrum collected with laser excitation at 785 nm (bottom raw). In blue are indicated Raman spectra obtained on the same sample but in different areas.

δC-H_2, and νC-C vibrations in ester groups, respectively (Table 4). These could have their origin in the presence of an organic coating in the analyzed area [37], probably applied during the restoration of the object. This information is consistent with the elevated Bal number of the p-XRF analysis of this object (Table 2), which indicates elements with a Z number lower than 12, such as C and H undetectable by this technique [24]. The same Raman bands, characteristic of an organic compound, are also observed for piece **1b**.

The Raman bands at 218 and 276 cm^{-1} observed in the shank of the ring **1a** (upper spectrum of Fig. 4, **1a Shank**) could be attributed to the presence of hematite (Fe_2O_3). Another Raman spectrum obtained on this object (lower spectrum in Fig. 4, **1a Shank**) also reveals the presence of bands at 303, 399, 554, and 684 cm^{-1} assigned to iron hydroxides, probably goethite (FeOOH) and/or magnetite (Fe_3O_4) [34,36].

Continuing with the analyses of iron-based objects, the spectrum of the **1d** Roman amulet is noteworthy, showing bands at 386 and 587 cm^{-1} assigned to vibrations of α-FeOOH and Fe_3O_4, respectively (Table 4), thus revealing a composition based on a mixture of iron hydroxides and oxides. Similarly, to the previously mentioned case of ring **1a**, amulet **1d** also presents bands at 217 and 276 cm^{-1}, which are assigned to vibrations of hematite [34]. The two broad bands around 1284 and 1584 cm^{-1} are due to the presence of amorphous carbon [36,38].

In the specific case of bead **1e**, Raman analyses were performed using two different laser excitation wavelengths, resulting in two distinct spectra. As illustrated in Fig. 4, **1e left**, the spectrum collected at 532 nm exhibits strong bands at 1129 and 1520 cm^{-1}, respectively assigned to νC-C and νC=C vibrations (Table 4). These are characteristic bands of a carotenoid pigment, the component responsible for the reddish-pinkish colour of the material. Addi-

Table 4
Summary of the main μ-Raman spectroscopy results. The samples from which the Raman signal could not be obtained are not included.

Sample	Laser excitation λ	Raman bands (cm^{-1})	Attribution	References
1a Shank	532 nm	218; 276	Hematite	[34–36]
		303; 399; 554; 684	Iron oxides	
1b Shank	532 nm	1108	C-C	[37]
		1452	C-H	
		1729	C=O	
1d	532 nm	217; 276	Hematite	[34–36,38]
		386	α-FeOOH (Goethite)	
		587	Fe_3O_4 (Magnetite?)	
		1284; 1584	Carbon-based materials	
1e	785 nm	284; 714; 1089	$CaCO_3$ (Calcite)	[39]
	532 nm	1129; 1520	C-C (Carotenoid pigment)	
1f	532 nm	570	Deformation and	[40]
		1093	stretching of SiO_4 groups	
		1113	C-CO	[37]
		1450	C-H	
		1731	C=O	
2a	785 nm	129; 208; 466	SiO_2 (α-Quartz) Moganite	[41,42]
		504		
2b	532 nm	129; 208; 466	SiO_2 (α-Quartz) Moganite	
		504		
4a	785 nm	1440	CH_2	[43,44]
		1604	C=C	
		2939	CH_2; CH_3	
7	532 nm	1388; 1600	Amorphous carbon	[38,39]

tionally, the spectrum of Fig. 4, **1e right**, collected at 785 nm, displays Raman bands of calcite ($CaCO_3$) at 284, 714 and 1089 cm^{-1}. In agreement with the work of reference [39] the assignment of bands of this object allows us to tentatively identify the material with red coral. Hasegawa, H. et al. [46] indicated that coral skeletons are mainly made of crystallized calcium carbonate ($CaCO_3$), along with other trace elements such as Mg, Sr, Fe, Al, and S. This composition is in agreement with the p-XRF and LIBS results (Tables 2 and 3, respectively) allowing us to conclude that the piece is made of red coral.

The intaglios **2a** and **2b** present the same clear μ-Raman bands of two silica polymorphs, as seen in Fig. 4**, 2a**. The two laser excitation wavelengths (532 and 785 nm) gave rise to spectra with matching bands at 129, 208, and 466 cm^{-1} attributed to alpha-quartz (α-SiO_2) vibrations. The band 466 cm^{-1}, which is the strongest of the whole spectrum, corresponds to SiO_4 six-membered ring vibration. The other two weaker bands at 129 and 208 cm^{-1} are assigned to Si-O-Si bending vibrations of microcrystalline α-SiO_2 and that at 504 cm^{-1} to symmetric stretching vibrations of the four-membered Si-O-Si ring of moganite (SiO_2). These two minerals that have the same composition but differ in crystallinity are distributed in different layers, forming agate [41,42], a material commonly used in Roman times.

Concerning the analyses of objects of carbon-based material composition, **1c, 3b, 4a, 4b, 5, 6**, and **7**, most of them did not present any Raman signal. Nonetheless, in the Visigoth **4a** bead, weak Raman bands were detected around 1450 and 1642 cm^{-1} (Fig. 3, 4**a**). These bands are the main ones in the range of 2000 to 1100 cm^{-1} attributed to the C–C stretching, and the deformation of CH_2 and CH_3 groups (Table 4), typical of amber [43,44]. Given that p-XRF and LIBS detected a high content of organic material, combined with the Raman results (Table 5), it can be concluded that these objects are made of amber. This material has been used for amulets and jewelry since Antiquity, due to its ease of carving and ancient societies' belief in its magical and medicinal properties [44,47].

On the other hand, the collected Raman spectrum on button **7**, shown in Fig. 3, revealed two broad bands around 1388 and 1600 cm^{-1}, characteristic of amorphous carbon [38,39]. These signals can be due to a jet gemstone (or black amber) [48]. Still, more carbonaceous sedimentary rocks, as presented in Hunter, et al. which display the same Raman bands as other carbon mineraloids (jet-like gemstones) like lignite or cannel coals [49]. Nevertheless, black amber has been used in personal adornment (beads, pendants, armlets, etc.) and artworks since ancient times to the present day. Furthermore, supported by p-XRF and LIBS results, exhibiting the same organoleptic characteristics, items **3b, 5**, and **6** are also likely manufactured from black amber (Table 5).

5. Conclusions

Based on the interdisciplinarity nature of the present research study, the results obtained reflect the complexity of the archaeological collections, especially in the case of personal adornment objects. The vast heterogeneity of materials employed to manufacture jewelry and/or apotropaic items has been demonstrated. Moreover, the investigation carried out provides valuable tools for historians and conservators, enabling them to link the use of these objects to various aspects of ancient societies, such as religious beliefs, funerary practices, commercial exchanges, and local manufacturing.

The information provided by the Museum catalog regarding the materiality of the objects was based on the organoleptic characteristics of the materials, and supported by the expertise of the conservators and archaeologists. For this reason, some of these objects were closely attributed to specific materials, while others remained unidentified.

The application of the considered multianalytical approach has proven useful in shedding light on these previously unknown materials. For instance, the proposed techniques have identified a variscite ($AlPO_4{\cdot}2(H_2O)$) intaglio of *La Loma del Regadío* Roman Villa, a singular material used in Antiquity, especially in Neolithic and Roman times; or the use of iron ore in the manufacture of an amulet found in *La Caridad* Roman site. In other cases, the analyses have significantly contributed to solving some of the uncertainties of the knowledge previously possessed by conservators. For instance, the intaglios from *El Palao* Ibero-Roman settlement, initially cataloged as quartz, have been confirmed by μ-Raman results to be agates. The stone-carved designs of these objects can be associated with typical styles of the Roman period of this site. Similarly, the pieces attributed to amber or black amber (jet), materials histori-

Table 5
Summary of the results from the multi-analysis carried out on the archaeological objects of personal adornment from the Museum of Teruel that led to the final identification of their material composition. Table 5. Summary of the analyses carried out on the archaeological objects for personal adornment of Teruel Museum. The table contains the main results of each analytical technique as taken from Table 2, Table 3, and Table 4. p-XRF considered results are the ones with values >0.1 wt % and Bal number >50.0 wt %. For LIBS, we have considered elements marked in bold in Table 3. The last column presents the final attribution to the specific material of each object.

Object		Archaeological site and date	Tentative attribution from museum catalog	Main p-XRF results (Bal values in wt %)	Main LIBS results	Main μ-Raman Spectrosc. results	Multianalytical study
1a Ring	Head	*La Caridad* site * - Late 2nd-c. BC - last third of 1st-c. BC	Unknown	Fe, Ca, Si, Bal (77.7)	Mo, Fe, Ca, Si	–	Glass paste
	Shank		Iron?	Fe	Fe	Mix of Fe oxides	Iron
1b Ring	Head		Unknown	Fe, Ca, Al, Si, Bal (68.0)	Mn, Ca, Si, Mg, Na	–	Glass paste
	Shank		Iron?	Fe	Mo, Fe	Organic coating	Iron
1c Cabochon			Amber?	High Bal (98.9)	Na, CN, C_2	–	Amber
1d Amulet			Unknown	Fe, Ca, K, Al, Si	Ba, Fe, Ca, Si	Mix of Fe oxides	Iron ore
1e Bead			Coral?	Ca, Si, Bal (74.3)	Sr, Ca, CaO, Mg	Calcite; carotenoid pigment	Coral
1f Cabochon			Glass paste?	Ca, Al, Si, Bal (62.0)	Mn, Ca, Si, Mg, Na	Glass; organic coating	Glass
2a Intaglio		Ibero-Roman settlement of *El Palao* - 2nd-c. BC - 1st-c. AD	Quartz?	Si, Bal (54.6)	Si	Quartz; Moganite	Agate
2b Intaglio			Quartz?	Si, Bal (62.0)	Si	Quartz; Moganite	Agate
3a Intaglio		Roman Villa of *La Loma del Regadío* - 3rd – 4th-c.	Unknown	Al, P, Si, Bal (78.3)	Cr, P, S, Al	–	Variscite
3b Bead			Black amber?	High Bal (91.0)	Sr, Ca, Mg, CN, C_2	–	Black amber
4a Bead		Hermitage of *La Virgen de la Peña* - Late 6th-c.	Amber?	High Bal (98.8)	Na, CN, C	C-C and CH groups	Amber
4b Bead			Amber?	High Bal (96.8)	Na, CN, C	–	Amber
5 Bead		Mausoleum of *Los Amantes de Teruel* - 13th-c.	Black amber?	High Bal (97.6)	Ca, CaO, CN	–	Black amber
6 Bead		Jewish necropolis of Teruel - 15th – 16th-c.	Black amber?	High Bal (96.6)	Sr, CN, C_2	–	Black amber
7 Button		*San Juan Bautista* Chapel - 18th-c.	Black amber?	High Bal (97.3)	Sr, Ca, CN, C_2	Amorphous carbon	Black amber

cally related to personal adornment and/or apotropaic or religious use, have been confirmed.

Additionally, the two rings produced by the iron industry provide evidence of the local production of metalworking production at *La Caridad* site, which was a significant economic driver for the settlement. Furthermore, the presence of a red coral bead suggests it may have been an object of commercial exchange, given its marine origin.

Finally, the present work has highlighted the tentative use of portable XRF equipment as a tool to characterize the materials and superficial deposits on these archaeological objects. Nonetheless, p-XRF results alone may not provide the most conclusive information for conducting the study of the material composition below the surface of the objects, especially considering the diverse materials found in personal adornment objects added to the drawbacks of this technique. Techniques such as LIBS and μ-Raman spectroscopy in their portable modality, even in a hybrid version [50], make the proposed methodology highly suitable for in situ analyses in museum collections or during archaeological excavation campaigns.

Acknowledgments

This research is partially funded by the E-RIHS.es Spanish node of E-RIHS (European Research Infrastructure for Heritage Science) through the CSIC Program for Large European Research Infrastructures 2022, grant INFRA20004, where access was provided by the Laser Laboratory for Heritage Science at Instituto de Química Física Blas Cabrera, with the collaboration of PetroLab (Petrophysic Laboratory, Geosciences Institute, CSIC). We also acknowledge the financial support from MCIN/AEI/10.13039/501100011033/FEDER, UE through the project PID2022-137017OB-I00 and Regional Government of Madrid through the project TEC Heritage-CM (TEC-2024/TEC-39), and the H2020 European project IPERION HS (Integrated Platform for the European Research Infrastructure ON Heritage Science, GA 871034). Support by the CSIC Platform "Open Heritage: Research and Society" (PTI-PAIS) and the CSIC Open Access Publication Support Initiative through its Unit of Information Resources for Research (URICI) are also acknowledged.

References

[1] S. Ridolfi, Portable X-ray fluorescence spectrometry for the analyses of cultural heritage, IOP Conf. Ser. Mater. Sci. Eng. 37 (2012) 012001, doi:10.1088/1757-899X/37/1/012001.
[2] J. Curran, T. Hicks, T. Trejos, Interpretation of glass evidence, in: V.J. Desiderio, C.E. Taylor, N.N. Daéid (Eds.), Handb. Trace Evid. Anal., John Wiley & Sons, Hoboken, NJ, USA, 2021, pp. 377–420.
[3] I. Liritzis, N. Zacharias, Portable XRF of archaeological artifacts: current research, potentials and limitations, in: M.S. Shackley (Ed.), X-Ray Fluoresc. Spectrom. XRF Geoarchaeology, Springer New York, New York, NY, 2011, pp. 109–142, doi:10.1007/978-1-4419-6886-9_6.
[4] L. Maestro-Guijarro, A. Pinilla, P.M. Carmona-Quiroga, F. Agua, M. Castillejo, M. García-Heras, M. Oujja, M.A. Villegas, Authentication of glass beads from Cultural Heritage: an interdisciplinary and multi-analytical approach, Talanta 286 (2025) 127510, doi:10.1016/j.talanta.2024.127510.
[5] L. Maestro-Guijarro, M. Sedano, N. Schibille, T. Pradell, M. Castillejo, M. Oujja, T. Palomar, Determination of boron content in surface paintings from historical stained-glass windows, Chemistry–Methods (2025) e202400057, doi:10.1002/cmtd.202400057.
[6] Edition of D. Anglos, V. Detalle, Cultural heritage applications of LIBS, in: S. Musazzi, U. Perini (Eds.), Laser-Induc. Breakdown Spectrosc. Theory Appl. Springer, Berlin, Heidelberg, 2014. Edition of.
[7] I. Donate, S. Díaz, E. García, M. Bueso, M. Martín, M. Oujja, M. Martínez-Weinbaum, M. Castillejo, LIBS vs XRF on underwater heritage: the silver coins of "Nuestra Señora de las Mercedes, in: Lasers Conserv. Artworks XIII, 1st ed., CRC Press, London, 2023, pp. 51–61, doi:10.1201/9781003386872-6.
[8] T. Palomar, M. Oujja, M. García-Heras, M.A. Villegas, M. Castillejo, Laser induced breakdown spectroscopy for analysis and characterization of degradation pathologies of Roman glasses, Spectrochim. Acta - Part B At. Spectrosc. 87 (2013) 114–120, doi:10.1016/j.sab.2013.05.004.
[9] T. Palomar, M. Oujja, M. Castillejo, R. Sabio, J.M. Rincón, M. García-Heras, M.A. Villegas, Roman glasses from Augusta Emerita: study of degradation pathologies using LIBS, Sci. Technol. Conserv. Cult. Herit. 45 (2013) 251–255, doi:10.1201/b15577.
[10] M. Oujja, M. Sanz, F. Agua, J.F. Conde, M. García-Heras, A. Dávila, P. Oñate, J. Sanguino, J.R. Vázquez De Aldana, P. Moreno, M.A. Villegas, M. Castillejo, Multianalytical characterization of Late Roman glasses including nanosecond and femtosecond laser induced breakdown spectroscopy, J. Anal. At. Spectrom. 30 (2015) 1590–1599, doi:10.1039/c5ja00150a.
[11] A. Martínez-Hernández, M. Oujja, M. Sanz, E. Carrasco, V. Detalle, M. Castillejo, Analysis of heritage stones and model wall paintings by pulsed laser excitation of Raman, laser-induced fluorescence and laser-induced breakdown spectroscopy signals with a hybrid system, J. Cult. Herit. 32 (2018) 1–8, doi:10.1016/j.culher.2018.02.004.
[12] A. Botto, B. Campanella, S. Legnaioli, M. Lezzerini, G. Lorenzetti, S. Pagnotta, F. Poggialini, V. Palleschi, Applications of laser-induced breakdown spectroscopy in cultural heritage and archaeology: a critical review, J. Anal. At. Spectrom. 34 (2019) 81–103, doi:10.1039/c8ja00319j.
[13] M. Oujja, F. Agua, M. Sanz, D. Morales-Martin, M. García-Heras, M.A. Villegas, M. Castillejo, Multiphoton excitation fluorescence microscopy and spectroscopic multianalytical approach for characterization of historical glass grisailles, Talanta 230 (2021) 122314, doi:10.1016/j.talanta.2021.122314.
[14] G.S. Senesi, O.D. Pascale, Laser-Induced Breakdown Spectroscopy (LIBS) in-situ: from portable to handheld instrumentation, in: S. D'Amico, V. Venuti (Eds.), Handb. Cult. Herit. Anal, Springer Nature, Switzerland AG, 2022, pp. 465–503.
[15] I.M.N. Ribeiro, R.P. Freitas, C. Calza, A.L.C. Oliveira, V.S. Felix, D.S. Ferreira, R.T. Batista, E.A.S. Gonçalves, M.O. Pereira, P.C.L. Brito, T.A. Lima, A.R. Pimenta, M.J. Anjos, R.T. Lopes, Analysis by Raman spectroscopy and XRF of glass beads from excavations in the harbor area of Rio de Janeiro, Brazil, Vib. Spectrosc. 87 (2016) 111–115, doi:10.1016/j.vibspec.2016.09.021.
[16] G. Ruello, A.A. Leonardi, D. Morganti, M.J. Lo Faro, A. Irrera, B. Fazio, Raman Spectroscopy, Methods and techniques for applications in cultural heritage, in: S. D'Amico, V. Venuti (Eds.), Handb. Cult. Herit. Anal., Springer International Publishing, Cham, 2022, pp. 560–579, doi:10.1007/978-3-030-60016-7.
[17] J.D. Vicente Redón, El Museo de Teruel, Antecedentes e historia breve de un museo provincial, Bol. Mus. Arqueol. Nac. Número Extraordin. 150 Años Mus. Arqueol. En Esp. 2 (2017) 513–527.
[18] J.D. Vicente Redón, B.Ezquerra Lebrón, La cultura material de La Caridad (Caminreal): un análisis preliminar, Treb. Arqueol. 25 (2023) 119–152, doi:10.5565/rev/tda.145.
[19] J.A. Benavente, F. Marco, P. Moret, El Palao de Alcañiz y el Bajo Aragón durante los ss. II y I a.C, Arch. Esp. Arqueol. Ser. Anejos 76 (2003) 231–246.
[20] S. Azuara Galve, C. Villargodo Ros, J. Pérez Arantegui, El complejo de prensado de la villa romana de la Loma del Regadío (Urrea de Gaén, Teruel), An. Prehist. Arqueol. 27–28 (2015) 219–230, doi:10.6018/apa.
[21] J.Á. Paz Peralta, La Antigüedad Tardía, Caesaraugusta 72 (1997) 171–274.
[22] J.R. Ayaso, Lápida sepulcral de Mosheh Najarí (Teruel), Miscelánea Estud. Árabes Hebraicos Sección Hebr. 67 (2018) 171–181. https://doi.org/10.30827/meahhebreo.v67i0.1012.
[23] A.C. Floriano Cumbreño, Hallazgo de la Necrópolis judáica de la ciudad de Teruel, Bol. Real Acad. Hist. Tomo 88 (1926) 845–851.
[24] R. López-Núñez, F. Ajmal-Poley, J.A. González-Pérez, M.A. Bello-López, P. Burgos-Doménech, Quick Analysis of Organic Amendments via Portable X-ray Fluorescence Spectrometry, Int. J. Environ. Res. Public. Health 16 (2019) 4317, doi:10.3390/ijerph16224317.
[25] National Institute of Standars and Technology, NIST atomic spectra database, (n.d.). https://www.nist.gov/pml/atomic-spectra-database (accessed October 21, 2024).
[26] S.S. Harilal, R.C. Issac, C.V. Bindhu, V.P.N. Nampoori, C.P.G. Vallabhan, Optical emission studies of species in laser-produced plasma from carbon, J. Phys. Appl. Phys. 30 (1997) 1703–1709, doi:10.1088/0022-3727/30/12/003.
[27] S.J. Mousavi, M. Hemati Farsani, S.M.R. Darbani, A. Mousaviazar, M. Soltanolkotabi, A. Eslami Majd, CN and C2 vibrational spectra analysis in molecular LIBS of organic materials, Appl. Phys. B 122 (2016) 106, doi:10.1007/s00340-016-6371-6.
[28] J.W. Anthony, R.A. Bideaux, K.W. Bladh, M.C. Nichols, eds., Variscite, in: Handb. Mineral., Mineralogical Society of America, Chantilly, VA 20151-1110, USA, (2001-2005) Mineral Data Publishing, version 1. https://www.handbookofmineralogy.org/pdfs/variscite.pdf (accessed December 30, 2024).
[29] Y. Abe, A. Nakamura, S. Suzuki, K. Tantrakarn, I. Nakai, J. Zöldföldi, P. Pfälzner, Use of variscite as a gemstone in the Late Bronze Age Royal Tomb at Qatna, Syria, J. Archaeol. Sci. Rep. 27 (2019) 101994, doi:10.1016/j.jasrep.2019.101994.
[30] S. Domínguez-Bella, Hispaniae Callais, The use of Iberian variscite in jewellery and mosaics in Roman times, in: G. Querré, S. Cassen, E. Vigier (Eds.), Parure En Callaïs Néolithique Eur, Archaeopress Publishing Ltd, Oxford, 2019, pp. 85–102, doi:10.2307/jj.15136071.
[31] Y.Díaz Acha, Caracterización de las Mineralizaciones de Gavà: Implicaciones Geoarqueológicas, Universitat de Barcelona, 2022.
[32] C.P. Odriozola, J.A. Linares-Catela, V. Hurtado-Pérez, Variscite source and source analysis: testing assumptions at Pico Centeno (Encinasola, Spain), J. Archaeol. Sci. 37 (2010) 3146–3157, doi:10.1016/j.jas.2010.07.016.
[33] G. Querré, T. Calligaro, S. Domínguez-Bella, S. Cassen, PIXE analyses over a long period: the case of Neolithic variscite jewels from Western Europe (5th–3th millennium BC), Nucl. Instrum. Methods Phys. Res. Sect. B Beam Interact. Mater. At. 318 (2014) 149–156, doi:10.1016/j.nimb.2013.07.033.
[34] M. Criado, S. Martínez-Ramirez, J.M. Bastidas, A Raman spectroscopy study of steel corrosion products in activated fly ash mortar containing chlorides, Constr. Build. Mater. 96 (2015) 383–390, doi:10.1016/j.conbuildmat.2015.08.034.

[35] G. Genchev, A. Erbe, Raman spectroscopy of Mackinawite FeS in anodic iron sulfide corrosion products, J. Electrochem. Soc. 163 (2016) 333–338, doi:10.1149/2.1151606jes.
[36] D.L.A. De Faria, F.N. Lopes, Heated goethite and natural hematite: can Raman spectroscopy be used to differentiate them? Vib. Spectrosc. 45 (2007) 117–121, doi:10.1016/j.vibspec.2007.07.003.
[37] P. Vandenabeele, L. Moens, H.G.M. Edwards, R. Dams, Raman spectroscopic database of azo and application to modern art studies, J. Raman Spectrosc. 31 (2000) 509–517, doi:10.1002/1097-4555(200006)31:6(509::AID-JRS566)3.0.CO;2-0.
[38] Z. Wang, C. Liu, G. Shi, G. Wang, H. Zhang, Q. Zhang, X. Jiang, X. Li, F. Luo, Y. Hu, K. Yi, Preparation and electrochemical properties of electrospun FeS/carbon nanofiber composites, Ionics 26 (2020) 3051–3060, doi:10.1007/s11581-020-03455-2.
[39] L. Bergamonti, D. Bersani, D. Csermely, P.P. Lottici, The Nature of the Pigments in Corals and Pearls: a Contribution from Raman Spectroscopy, Spectrosc. Lett. 44 (2011) 453–458, doi:10.1080/00387010.2011.610399.
[40] A. Tournié, L.C. Prinsloo, P. Colomban, Raman classification of glass beads excavated on Mapungubwe hill and K2, two archaeological sites in South Africa, J. Raman Spectrosc. 43 (2012) 532–542, doi:10.1002/jrs.3069.
[41] X. Li, H. Xue, X. Wu, D. Qin, D. Chen, J. Yuan, Z. Tang, Artificial coloration of ancient agate beads: a mineralogical study, Herit. Sci. 11 (2023) 195, doi:10.1186/s40494-023-01039-7.
[42] J. Götze, K. Stanek, G. Orozco, M. Liesegang, T. Mohr-Westheide, Occurrence and distribution of moganite and opal-CT in Agates from Paleocene/Eocene Tuffs, El Picado (Cuba), Minerals 11 (2021) 531, doi:10.3390/min11050531.
[43] B.I. Łydżba-Kopczyńska, B. Gediga, J. Chojcan, M. Sachanbiński, Provenance investigations of amber jewelry excavated in Lower Silesia (Poland) and dated back to Early Iron Age, J. Raman Spectrosc. 43 (2012) 1839–1844, doi:10.1002/jrs.4187.
[44] A. Rygula, A. Klisińska-Kopacz, P. Krupska-Wolas, T. Wilkosz, M. Matosz, M. Obarzanowski, K. Skóra, A. Kopyciak, J.M. Del Hoyo-Meléndez, Detection of protective coatings applied on baroque amber artworks: case studies, Heritage 7 (2024) 4109–4130, doi:10.3390/heritage7080193.
[45] P. Colomban, A. Tournie, L. Bellot-Gurlet, Raman identification of glassy silicates used in ceramics, glass and jewellery: a tentative differentiation guide, J. Raman Spectrosc. 37 (2006) 841–852, doi:10.1002/jrs.1515.
[46] H. Hasegawa, M.A. Rahman, N.T. Luan, T. Maki, N. Iwasaki, Trace elements in Corallium spp. as indicators for origin and habitat, J. Exp. Mar. Biol. Ecol. 414–415 (2012) 1–5, doi:10.1016/j.jembe.2012.01.005.
[47] G.N. Gestoso Singer, Amber exchange in the Late Bronze Age Levant in cross–cultural perspective, Aula Orient. Rev. Estud. Próximo Oriente Antig. 34 (2016) 254–264.
[48] A. Demény, M. Bondár, M. Karlik, I. Hegyi, I. Gábor Hatvani, A.R. Facsády, K. Csontos, A. Gugora, R. Kara-Gülbay, J. Carlos García-Ramos, S. Caldwell Steele, Provenance groups in a Roman jet jewelry collection at Aquincum (Budapest, Hungary) and comparison with jet and jet-like gemstones, J. Archaeol. Sci. Rep. 54 (2024) 104413, doi:10.1016/j.jasrep.2024.104413.
[49] F.J. Hunter, J.G. McDonnell, A.M. Pollard, C.R. Morris, C.C. Rowlands, The scientific identification of archaeological jet-like artefacts, Archaeometry 35 (1993) 69–89, doi:10.1111/j.1475-4754.1993.tb01024.x.
[50] A. Nevin, G. Spoto, D. Anglos, Laser spectroscopies for elemental and molecular analysis in art and archaeology, Appl. Phys. A 106 (2012) 339–361, doi:10.1007/s00339-011-6699-z.